electronics

MDPI

Article

Entropy-Based Low-Rank Approximation for Contrast Dielectric Target Detection with Through Wall Imaging System

Mandar Bivalkar [1], Dharmendra Singh [1,*] and Hirokazu Kobayashi [2]

[1] Indian Institute of Technology Roorkee, Roorkee, Uttarakhand 247667, India; mbivalkar@somaiya.edu
[2] Osaka Institute of Technology Osaka, Osaka Prefecture 535-8585, Japan; hirokazu.kobayashi@oit.ac.jp
* Correspondence: dharmfec@gmail.com

Received: 29 April 2019; Accepted: 30 May 2019; Published: 5 June 2019

Abstract: In through wall imaging, clutter plays an important role in the detection of objects behind the wall. In the literature, extensive studies have been carried out to eliminate clutter in the case of targets with the same dielectric. Existing clutter reduction techniques, such as the sub-space approach, differential approach, entropy-based time gating, etc., are able to detect a single target or two targets with the same dielectric behind the wall. In a real-time scenario, it is not necessary that targets with the same dielectric will be present behind the wall. Very few studies are available for the detection of targets with different dielectrics; here we termed it "contrast target detection" in the same scene. Recently, low-rank approximation (LRA) was proposed to reduce random noise in the data. In this paper, a novel method based on entropy thresholding for low-rank approximation is introduced for contrast target detection. It was observed that our proposed method gives satisfactory results.

Keywords: through-wall imaging; contrast target detection; clutter reduction; entropy thresholding; low-rank approximation

1. Introduction

Through wall imaging (TWI) is emerging as an important technology for surveillance, security and rescue missions. The main aim of TWI is seeing through a wall with the help of electromagnetic waves. In any radar system, the signal-to-clutter ratio (SCR) plays an important role in the improvement of the detection of the objects. The SCR can be improved either by classical or statistical methods [1]. Classical methods use different classical digital filters, while statistical methods exploit the statistical nature of the received signal to separate the clutter from the signal.

Digital filtering technique [2] uses frequency analysis of the clutter geometrical model and the signal geometrical model, while in [3], the coupled iterative procedure was used to reduce the ground reflections for the application of ground penetrating radar (GPR). The classical clutter reduction algorithm (CCRA) was proposed in [4,5], but this method does not optimize the coefficients for the representation of noise and the target. Kalman filtering uses the background component model in [6], but designing the Kalman filter is computationally intensive. Parametric clutter reduction was proposed in [3] by modeling the variations in the received signal, but it requires a reference signal, which cannot practically be made available.

In the literature, various statistical clutter reduction techniques have been proposed. Different statistical reduction techniques were compared in [7]. Verma et al. [1] applied various statistical techniques for clutter reduction such as singular value decomposition (SVD), principle component analysis (PCA), factor analysis (FA), and independent component analysis (ICA), and concluded that ICA performs better for the detection of low dielectric material behind a wall.

The major contribution to the clutter in TWI is due to reflections from the wall. Different wall removal techniques are proposed in the literature, such as the sub-space projection approach that is used in [8] for wall removal. SVD frequently using the sub-space projection approach for clutter reduction, and it has previously been used to enhance the signal-to-clutter ratio for the application of ground penetrating radar (GPR) [9] and TWI in [10]. In SVD, Eigen-images of the B-scan are determined and used to identify wall clutter and target subspace. In [11], it is stated that the first two Eigen-values correspond to the wall and target, respectively, but [8] shows that wall clutter is spread along with the high dimensional subspace and weak wall singular components interleave with target subcarriers. Recently, the empirical low- rank approximation method was proposed in [12] for seismic data, where all Eigen-values corresponding to the noise subspace were considered to identify the weak signals. If we consider all the Eigen-values along with the Eigen-values corresponding to the signal, then noise is also get added in the signal.

Compared to other imaging systems such as GPR and biomedical, TWI has to deal with more severe problems like changes in the propagation environment and sensor positioning [13,14]. Another problem in TWI is the propagation medium, where multiple unknowns and either homogenous or non-homogenous walls are involved [15]. In a real-time scenario, it may be possible that targets with different dielectrics will be present behind the wall. It is challenging to detect low dielectric targets such as wood ($\approx$4) in the presence of metal ($\approx\infty$) behind the wall because in TWI images, low dielectric targets are obscured in the presence of high noise. We termed the target detection and imaging problem in which targets with different dielectrics are present as "contrast target detection" and "contrast target imaging", respectively. The contribution of this paper is that first we propose a novel method to detect contrast targets using a sub-space projection approach based on low rank approximation (LRA) and modify it using entropy in the Eigen-values to reduce the clutter from the useful signal. Second, we solve the inherent problem of considering a large rank for the signal recovery in LRA by introducing an entropy-based threshold. The critical analysis of existing clutter reduction techniques shows that they cannot detect contrast targets in the scene. The performance of the proposed method is compared with other traditional techniques such as an average trace subtraction, subspace projection, entropy based time gating, SVD, ICA and the differential approach for the targets having contrast dielectrics.

The remainder of this paper is organized as follows. Geometry for the TWI imaging is presented in Section 2. Different clutter reduction techniques are presented along with the results in Section 3. Novel methods for entropy-based low-rank approximation for contrast imaging is proposed in Section 4. Section 5 concludes the paper.

2. TWI Data Collection and Beamforming

2.1. Data Collection

Data is collected by placing different dielectric materials such as metal or wood behind the wall at different distances in our experimental work. Synthetic aperture radar (SAR) in the multi-static mode in which an array of antennas are used to scan the whole wall at M different locations, and the reflection coefficient (S11) is measured for P- targets in the scene using system parameters given in Table 1 and then set-up, which is shown in Figure 1. Received frequency domain data is converted to time domain [16]

Step (1): Transformation from Time domain to spatial domain

Time domain signal is converted to spatial domain to determine the range profile by using $z = c * t/2$ where c is the speed of light and t is a delay.

Step (2): External calibration

The metallic plate is placed in front of the antenna [17] to find the delay due to the antenna system, which will be subtracted from the observed data. The range profile is corrected using the difference in the delay.

Step (3): Velocity correction

As the antenna is placed at the standoff distance from the wall, the signal propagates through the air, then the wall and again through the air up to the target. The presence of the wall scattered the signal, and shifting of the target position took place. This shifting was compensated using the method of velocity correction. The mathematical equation for this is given next in the paper.

Table 1. System parameters.

Sr. No.	Parameters	Value
01	Radar type	SFCW
02	Frequency range	1 GHz–3 GHz
03	Transmitted power	3 dBm
04	Number of frequency points	201
05	Bandwidth	2 GHz
06	Cross-range resolution	15 cm
07	Down-range resolution	7.5 cm
08	Polarization	VV
09	Antenna type	Horn
10	Gain of Antenna	20 dB
11	Beam-width	15.92° and 17.02°

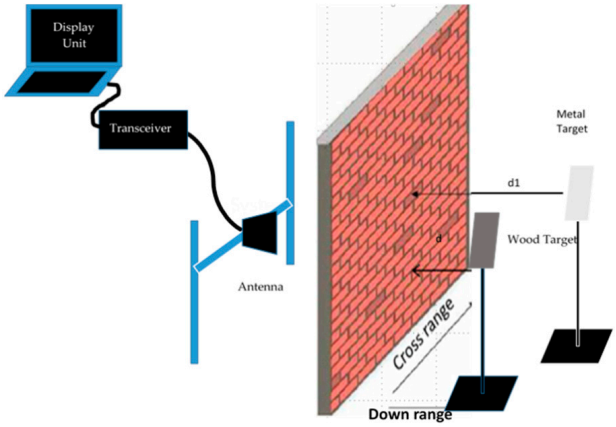

Figure 1. Through Wall Imaging (TWI) set- up.

2.2. Beamforming

The antenna is placed in front of the wall at a fixed standoff distance and data is collected for M different locations that received the signal, represented as Equation (1).

$$x(n,t) = \sum_{p=0}^{P-1} \sigma_p s(t - \tau_{n,p}) \tag{1}$$

where $s(t)$ is the transmitted signal convolved with the transfer function of the wall [14] for the SFCW radar. σ_p is the reflection coefficient, and $\tau_{n,p}$ is the two-way delay—the time between the n^{th} antenna position and the target P. When the signal propagates between the n^{th} antenna positions and p^{th} target, the two-way delay-time is given as Equation (2)

$$\tau_{n,p} = \frac{2}{c}\sqrt{(x_p - x_n)^2 + (y_p - y_n)^2} \tag{2}$$

where c is the speed of light.

In this paper, the focused image has been developed using DS (delay-and-sum) beamforming for collected data. The i^{th} pixel value in the DS image is given by Equation (3)

$$b(i,j) = \frac{1}{N}\sum_{n=o}^{N-1} x(n, t + \tau_n(i,j)) \tag{3}$$

where $\tau_n(i,j)$ is the propagation delay on both sides of the wall. The SFCW radar, for which stepped size depends upon the selection of frequency bins, requires trade-off between a number of frequency bins and scanning time. The SFCW radar waveform consists of Q- narrowband signals defined as Equation (4)

$$b(i,j) = \sum_{n=o}^{N-1}\sum_{q=o}^{Q-1} x(n, f_q) \tag{4}$$

where $x(n, f_q)$ is the signal received at the n^{th} antenna position for the frequency q.

S11 data is collected either in the time domain or frequency domain [18]. We collected data for three targets with different dielectrics by arranging them at different positions behind the wall (refer to Appendix A). Our method was tested on collected data for illustration purposes, with a few results given in Sections 3 and 4. The geometry for the TWI is shown in Figure 2, if we consider the point target at X_p, then developing the image transformation is required from the time to the spatial domain.

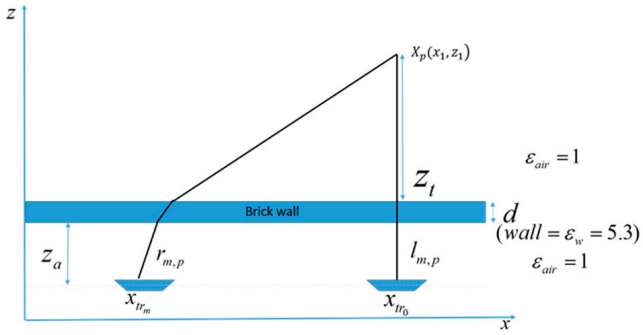

Figure 2. Through Wall Imaging (TWI) Geometry.

Delay-sum-beamforming is the most popular and least complex imaging algorithm, interested readers may refer to [19] for more details. The signal received at the antenna location is $z[m,q]$ of the frequency f_n with a delay $\tau_{p,m}$, then $z[m,q]$ can be represented as Equation (5)

$$z[m,q] = \sum_{p=0}^{P-1} \sigma_p \exp\{-j2\pi f_n \tau_{p,m}\} \tag{5}$$

where m and $\boldsymbol{q}$ represents the spatial index and frequency index, respectively. In our experimental set-up, we considered a homogenous wall of thickness d = 15 cm and relative permittivity of the wall of $\varepsilon_w = 5.3$. The dielectric constant of the wall is measured as described in [20]. The distance from the antenna to the wall is (z_a) and from a wall to the target is (z_t). The velocity correction [21] for geometry shown in Figure 2 is given by Equation (6)

$$d_v = z_a + d\sqrt{\varepsilon_w} + z_t \tag{6}$$

where d_v is the actual distance between the antenna and the target after velocity correction. $\tau_{n,p}$ can be estimated by putting Equation (6) into Equation (2)

$$\tau_{n,p} = \sqrt{(x_{tr_0} - x_{tr_n})^2 + (d_v + X_p)^2} \tag{7}$$

We can recover the image $s[k,l]$ by DS–beamforming using Equation (8)

$$s[x_k, z_l] = \frac{1}{MQ}\sum_{m=0}^{M-1}\sum_{q=0}^{Q-1} z[m,q]\exp\{j2\pi f_n \tau_{n,p}\} \tag{8}$$

where k and l are the number of pixels in the image.

3. Clutter Reduction Techniques

Clutter is the unwanted reflections due to other objects in the room. Clutter overwhelms the target, and so clutter reduction techniques can be used to separate clutter from the target. The data collected for the n^{th} observation can be denoted as

$$s(t) = s_a(t) + s_w(t) + s_p(t) \tag{9}$$

where $s_a(t)$ are the reflections due to an antenna mismatch, $s_w(t)$ are the reflections due to the wall and $s_p(t)$ are the contribution due to p (the number of targets behind the wall). The discrete form of collected data for M antenna locations at N different instances can be arranged in an $M \times N$ data matrix.

$$s = [s_0, s_1, \ldots, s_{M-1}] \tag{10}$$

We try to separate the $s_p(t)$ signal from $s_a(t)$ and $s_w(t)$ using clutter reduction methods [22].

Imaging for raw data was done with the help of DS beamforming as discussed in Section 2. Raw normalized images for different targets after pre-processing are shown in Figure 3. It can be seen from the DS images for different targets, along with the target, clutter due to the wall and other objects also dominate, which may obscure the target. The reflections from the low dielectric targets are generally weak compared to clutter from the interior and exterior of the wall, making detection of such targets difficult. Efficient clutter reduction technique is required to remove the clutter from the B-scan image to detect low dielectric targets [23]. After pre-processing, different commonly used clutter reduction techniques are implemented and the results of this are discussed here. Their performance is given in terms of the PSNR (peak signal-to-noise ratio) [24].

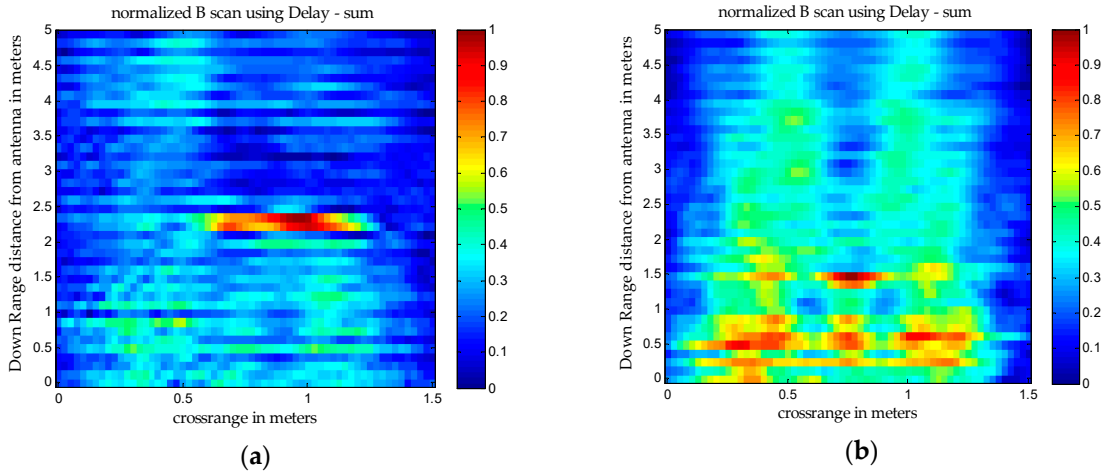

(**a**) (**b**)

Figure 3. *Cont.*

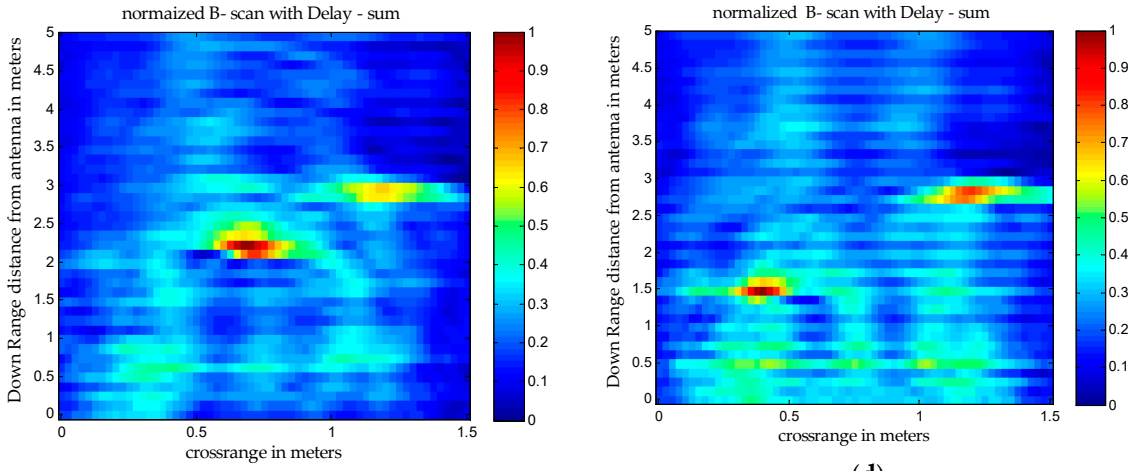

Figure 3. Delay and Sum B-scan images (**a**) Target ID 01: Metal target, (**b**)Target ID 02: Wood target, (**c**) Target ID 05: Two metal targets, (**d**)Target ID 07: Metal and wood targets where color bar represents normalized intensity value.

3.1. Average Trace Subtraction

In general, clutter remains constant with respect to target reflections for data collected [25], hence we can consider that clutter will be constant for a homogenous wall. We can separate a constant signal from the non-constant signal using spatial filtering [26] in the time domain, which can be represented as

$$\begin{array}{c} s_{av}(n,m) = s(n,m) - \bar{s}(m) \;\; m = 0 \ldots M-1 \\ \text{Where } \bar{s}(m) = \frac{1}{N}\sum_{n=0}^{N-1} s(n,m) \;\; m = 0 \ldots M-1 \end{array} \tag{11}$$

where $s(n,m)$ is the data matrix element and $\bar{s}(m)$ is the average of the data matrix. The Fourier transform for (11) can be given as

$$\begin{array}{l} \widehat{s}_{av}(k_x,m) = \sum_{n=0}^{N-1} s_{av}(n,m)\exp(-ik_x n\Delta x)\Delta x \\ = \widehat{s}(k_x,m) - \bar{s}(m)\frac{\sin(N\Delta x k_x/2)}{\sin(\Delta x k_x/2)} * \exp[-i\Delta x k_x(N-1)/2] \end{array} \tag{12}$$

where k_x represents spatial frequency ($\Delta x \leq 2\pi/k_0$), and k_0 is the frequency wave number. This condition cover [$-k_0$,k_0] and no filtering is introduced by the grating lobe. Due to the Dirichlet condition appearing in Equation (12), the low-frequency spatial spectrum of target signal s_n will also get rejected, and due to this target which is placed near the wall, cannot be detected.

3.2. Differential Approach

In this approach the clutter is removed by subtracting the adjacent two traces [27], for the time domain data this is represented as [28]

$$s_{DA}(n,m) = s(n+1,m) - s(n,m) \;\; m = 0 \ldots\ldots M-1, \; n = 0 \ldots\ldots N-2 \tag{13}$$

The corresponding spatial spectrum can be given as

$$\widehat{s}_{DA}(k_x,m) \simeq 2j\widehat{s}(k_x,m)(\sin(\frac{k_x\Delta x}{2})) \tag{14}$$

The observation point corresponds to $x_n = (n+1/2)\Delta x$ $n = 0, \ldots, N-1$ and $n = 0, \ldots, N-2$ in the first and second term. It can be seen from Equation (14) that de-cluttering can be achieved locally

and that not all traces are exploited simultaneously. If Δx is very small, then the **sin** term rises very slowly, and if it is very high, then artifacts corrupt the reconstruction.

3.3. Subspace Projection Approach

Subspace approaches are used to separate out complementary subspaces, called the target and clutter, in order to increase SCR. In the literature, many methods for clutter reduction using the subspace projection approach are given. Here we will restrict our discussion to SVD and ICA.

3.3.1. Singular Value Decomposition (SVD)

SVD is the most efficient technique from linear algebra for clutter reduction. SVD decomposition of the B-scan matrix (S) of dimension $M \times N$ is given by

$$S = UDV^T \tag{15}$$

where $U = [U_1, U_2, \ldots, U_M]$ and $V = [V_1, V_2, \ldots, V_N]$ are the left and right singular matrix whose column are Eigen-vectors. The D matrix is the diagonal matrix for which singular values are arranged in decreasing order. The B-scan matrix for SVD of S is given by

$$S = \sum_{i=1}^{N} w_i u_i {v_i}^T \tag{16}$$

where $u_i {v_i}^T$ are the Eigen-component and w_i is the Eigen-value for the i^{th} component. The first Eigen-value represents the strong reflections, which are generally from the wall in the case of TWI, the remaining values represent other reflections from the target and noise. We can categorize Eigen-space into target sub-space and noise sub-space. Let $E_i = u_i {v_i}^T$ then

$$E = [E_{1\to k} \big| E_{k+1\to p} \big| E_{p+1\to N}] \tag{17}$$

where $E_{1\to k}$ represents strong reflections, $E_{k+1\to p}$ represents reflections from the target and $E_{p+1\to N}$ represents noise.

3.3.2. Independent Component Analysis (ICA)

ICA divides the data into statistically independent components. Statistical independence considers higher order moments for data matrix $\boldsymbol{S}$. ICA takes a linear combination of $\boldsymbol{S_x}$ such that

$$I_x = \sum_{j=1}^{N} a_{ij} s_j \quad j = 1, 2, \ldots NI = SA \tag{18}$$

where $\boldsymbol{A}$ is the matrix holding N independent source components. The output signal matrix $\boldsymbol{Y}$ is for the input matrix, matrix $\boldsymbol{I}$ can be determined with the help of the full rank matrix ($\boldsymbol{W}$), such that

$$Y = WI \tag{19}$$

where $\boldsymbol{W}$ is the matrix which makes $\boldsymbol{I}$ as independent as possible for dependent sensor signals $\boldsymbol{S}$.

3.4. Entropy-based Time Gating

Recently in [25], entropy-based time gating was proposed for clutter reduction, and it is shown that this method is efficient for clutter reduction compared to earlier methods in the literature. In this method behavior of the clutter, which is similar over each time trace, is used to exploit the entropy.

Clutter signal gives higher entropy compared to the target. The threshold set in this paper is as Equation (20)

$$W(m) = 0 \text{ if entropy } \geq \alpha \log(N-1) \text{ and} W(m) = 1 \textit{ elsewhere} \quad (20)$$

where $\alpha < 1$ is the tolerance for the threshold and N is the number of scanning points

The time trace after incorporating the threshold is given as

$$e_w(n,m) = W(m)e(n,m) \quad (21)$$

To illustrate the results using the above methods, we used the data collected with a single metal target and two targets of metal and wood for contrast imaging as described in Section 2. The PSNR for each method in both cases is given in Tables 2 and 3.

Table 2. PSNR in dB for Metal target.

Sr. No.	Clutter Reduction Method	PSNR in dB
1.	Average trace subtraction	10.7504
2.	Singular value decomposition	7.6220
3.	Differential approach	10.1494
4.	Independent component analysis	12.6255

Table 3. PSNR in dB for Metal and wood.

Sr. No.	Clutter Reduction Method	PSNR in dB
1.	Average trace subtraction	9.9608
2.	Singular value decomposition	9.8052
3.	Differential approach	9.3390
4.	Independent component analysis	12.8549

It can be seen from Figure 4 that both targets are visible along with some clutter by using average trace subtraction, but they are not visible by other methods. It is necessary to develop an efficient clutter removal technique to detect a weak target in the presence of the strong clutter.

PSNR is the ratio to analyze the distortion in the final image with respect to the input low-resolution image is given by

$$PSNR = 10 \log_{10} \frac{1}{MSE} \quad (22)$$

$$MSE = \frac{(O.I. - F.I.)^2}{(V.P. * H.P.)} \quad (23)$$

where

MSE—Mean square error
O.I.—Original normalized image
F.I.—Final image
V.P.—Number of vertical scanning points
H.P.—Number of horizontal scanning points

It can be observed from Tables 1 and 2, the PSNR for ICA is high among all other clutter reduction techniques. Even if ICA is efficient for the detection of the low dielectric target it cannot detect a wood target when it is placed at a different down range position compared to the metal target.

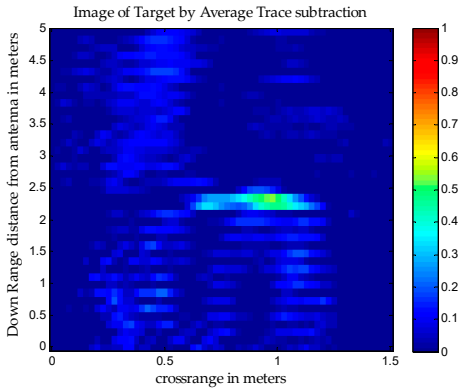

(**a**) Target ID 01

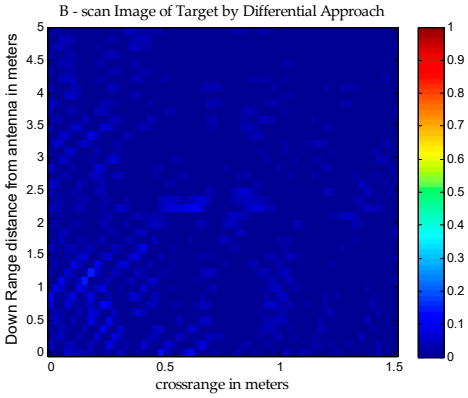

(**b**) Target ID 01

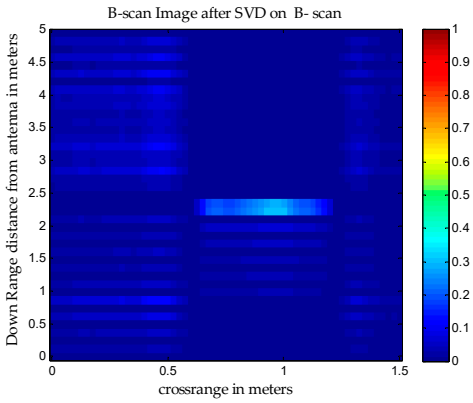

(**c**) Target ID 01

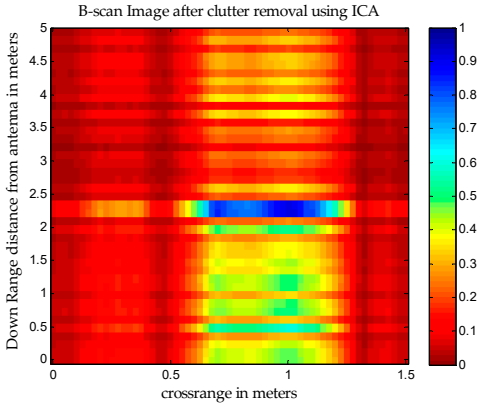

(**d**) Target ID 01

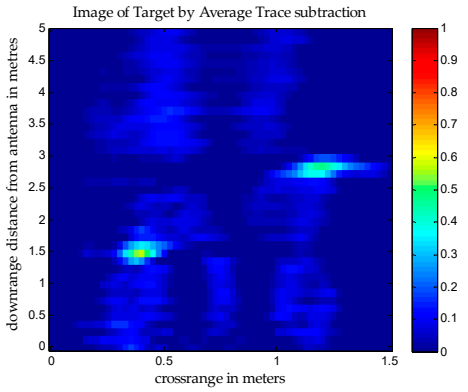

(**f**) Target ID 07

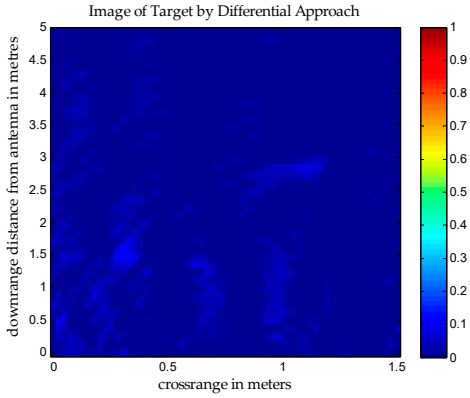

(**g**) Target ID 07

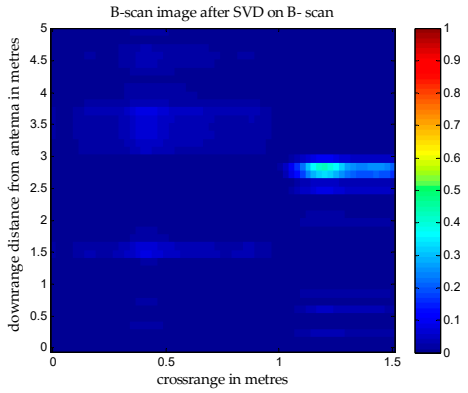

(**h**) Target ID 07

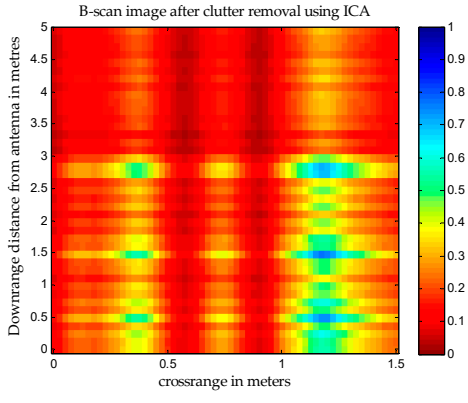

(**i**) Target ID 07

Figure 4. *Cont*.

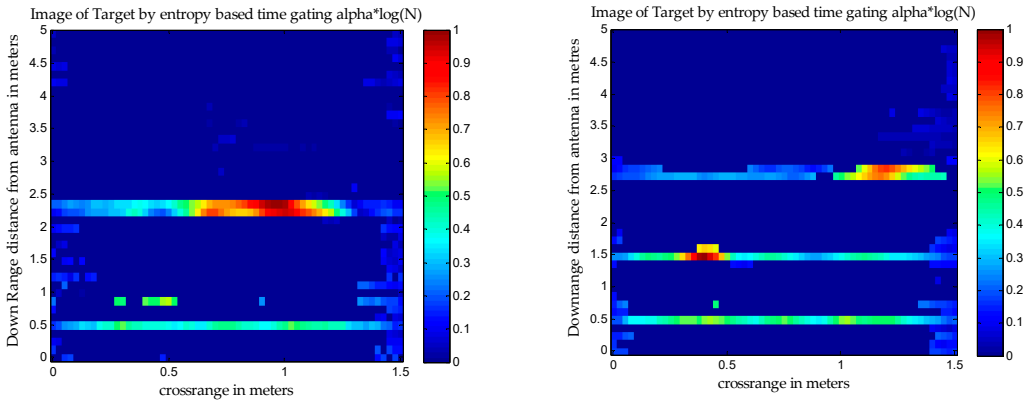

(**e**) Target ID 01 (**j**) Target ID 07

Figure 4. B-scan images. (**a**) Average trace subtraction for metal target; (**b**) Differential approach for metal target; (**c**) SVD for metal target; (**d**) ICA for metal target; (**e**) Entropy-based time gating for metal target; (**f**) Average trace subtraction for metal and wood targets; (**g**) Differential approach for metal and wood targets; (**h**) SVD for metal and wood targets; (**i**) ICA for metal and wood targets; (**j**) Entropy-based time gating for metal and wood targets where color bar represents normalized intensity values.

4. A Proposed Novel Method for Contrast Imaging

Low-rank approximation (LRA) has been used recently for seismic data [12]. LRA is efficient compared to SVD and ICA as it exploits the noise space by considering the large rank, this motivates us to use LRA for the detection of contrast targets. LRA is a rank reduction technique, the principle requirement of the LRA is that the data should be low rank. In TWI imaging, the number of targets are less than the number of scanning points ($P < MN$), hence the collected data is inherently sparse and low rank. Steps for traditional LRA are

Step (1): Calculate the SVD for data matrix S.

$$S = U * D * V^T \tag{24}$$

Step (2): Select n largest diagonal singular values from the matrix D and set other values to zero.

$$\widehat{D} = D(1:n, 1:n) \tag{25}$$

Step (3): Calculate the LRA matrix.

$$\widehat{S} = U\widehat{D}V^T \tag{26}$$

While selecting the n largest singular or Eigen-values from matrix D, we ignore the first Eigen-value, which represents the strongest reflections from the wall [1]. The modified LRA for TWI can be given as

Step (4): Ignore first Eigen-value corresponding to wall reflections, hence the matrix D is given as

$$\widehat{D} = D(2:n, 2:n) \tag{27}$$

To satisfy the principle of the algorithm, LRA works in the local windows, where deciding the optimum rank is difficult. Since LRA cannot estimate the optimum rank in the local window, it will consider the large rank to preserve the useful energy in the signal. In the attempt to preserve the useful energy using the large rank, unwanted clutter is also added to the signal. This problem can be solved by using an optimum threshold while selecting Eigen-values during the reconstruction of the useful signal.

Step (5): Select the optimum threshold for Eigen-values from LRA using the entropy-based criterion.

We used the entropy-based criterion [25] for selecting the threshold for the Eigen-values in the LRA. The idea for entropy-based thresholding was adapted to discriminate between target and clutter signals. To select the optimum threshold, we consider the criteria that entropy is maximum for clutter and minimum for the target. First, we construct the normalized time traces as

$$S_{Nz}(n,m) = \frac{S(n,m)^2}{\sum_{l=0}^{N-1} S(l,m)^2} \quad m = 0, 1, \ldots, M-1 \tag{28}$$

$$\text{Now } S_{Nz}(n,m) \geq 0 \text{ and } \sum_{n=0}^{n-1} S_{Nz}(n,m) = 1 \text{ for all } m \tag{29}$$

At each instant, normalized data is considered to be a probability density function (PDF) [29]. Introducing PDF allows us to adopt the entropy-based criterion to determine the threshold and entropy measure, which is given as

$$E_S(m) = -\sum_{n=0}^{N-1} S_{Nz}(n,m) \log(S_{Nz}(n,m)) \tag{30}$$

The entropy of the clutter signals gives large values and the clutter in the observations is generally constant, hence the average value for the Eigen-values can be the optimum threshold. The flow chart for the proposed method is given in Figure 5.

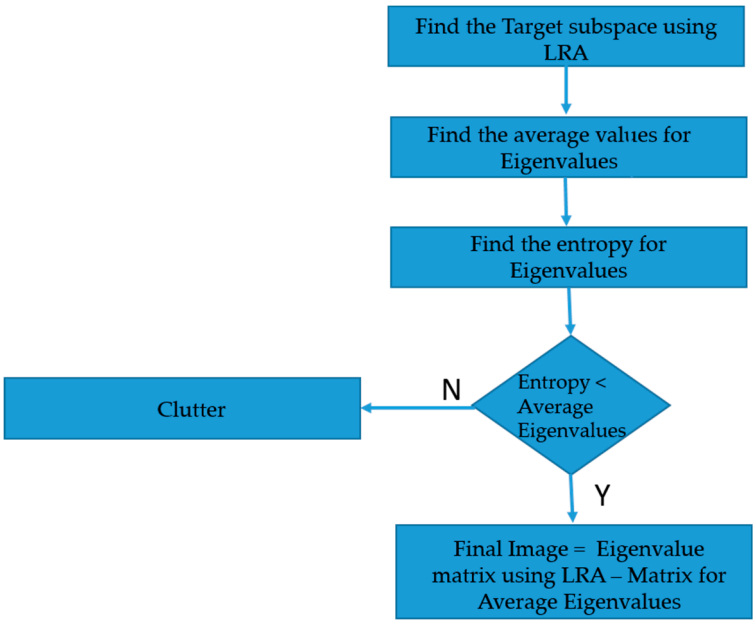

Figure 5. Flow chart for the proposed method.

For subspace approaches, such as SVD and ICA, only a few dominant Eigen-values are considered as the target and lower Eigen-values are considered as the noise, as a result, weak targets are considered as noise. In the proposed developed method, we consider all the Eigen-values and set the optimum threshold to eliminate the noise–space, hence we are able to detect weak targets such as wood along with a strong target such as metal.

The data is processed with different targets to check the capability of the method. For contrast imaging, two targets with different dielectrics are chosen behind the wall, i.e., metal and wood. The results for which are shown in Figure 6.

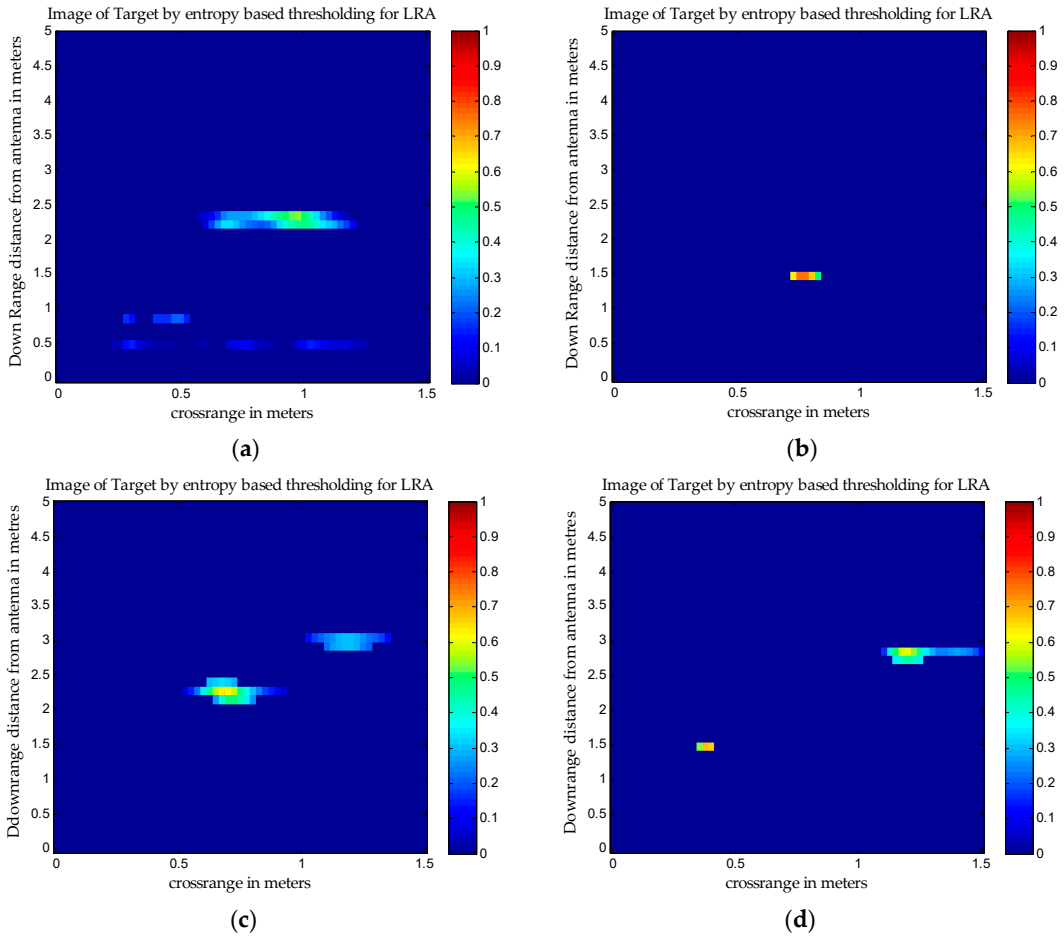

Figure 6. B- scan images with a proposed method with (**a**) Target ID 01: single metal target, (**b**) Target ID 02: single wood target, (**c**) Target ID 05: Two metal targets, (**d**) Target ID 07: Metal and wood targets where color bar represents normalized intensity values.

5. Conclusions

In this paper, the problem of contrast imaging is addressed and it is shown that our developed method is able to detect a weak target in the presence of a strong target. The inherent problem of considering the large rank in LRA is solved by setting the optimum threshold using the entropy-based criterion. The entropy-based LRA method was compared to other methods, such as *average trace subtraction*, *entropy-based time gating*, *SVD*, *ICA* and *DA*, and found to be very effective for different types and arrangements of the target.

Another advantage of the proposed method is that it also avoids the filtering of low spatial targets and therefore this method allows a better reconstruction of low as well as high dielectric targets in the scene. In our future work, we are going to work on rank optimization problem of LRA.

Author Contributions: Conceptualization, Experimental details, D.S.; Supervision, D.S.; Writing—original draft, Experimental work, M.B.; Writing—review & editing, D.S. and H.K.

Funding: This research received no external funding.

Conflicts of Interest: The authors declare no conflict of interest.

Appendix A

We collected 45 datum points for different arrangements of a target position behind the wall, target size and target thickness. The distance of the target is measured from the antenna mouth. Table 3

gives target types while Figures A1–A3 gives A-scan, B-scan and C-scan images using the proposed method as described in Section 4, which are given for validation.

Table A1. Types of targets.

Target ID	Number of Targets	Target Type	The Distance of the Targets from the Antenna Mouth	Target Size/Thickness
01	01	Metal	2.3 m	17.5 cm × 14.5 cm/1 cm
02	01	Wood	1.5 m	Thick wood: 50 cm × 30 cm/2 cm Thin wood: 30 cm × 30 cm/1 cm
03	01	Teflon	1.5 m	50 cm × 40 cm/1 cm
04	02	Metal-Metal	3 m	17.5 cm × 14.5 cm/1 cm
05	02	Metal-Metal	2.3 m and 3 m	17.5 cm × 14.5 cm/1 cm
06	02	Metal-Wood	1.73 m	17.5 cm × 14.5 cm/1 cm, Thick wood: 50 cm × 30 cm/2 cm
07	02	Metal-Wood	2.3 m and 1.5 m	17.5 cm × 14.5 cm/1 cm, Thick wood: 50 cm × 30 cm/2 cm
08	02	Metal-Teflon	2.3 m	17.5 cm × 14.5 cm/1 cm, 50 cm × 40 cm/1 cm
09	02	Metal-Teflon	2.3 m and 1 m	17.5 cm × 14.5 cm/1 cm, 50 cm × 40 cm/1 cm
10	02	Wood (thick)–Wood (thin)	1.73 m	Thick wood: 50 cm × 30 cm/2 cm Thin wood: 30 cm × 30 cm/ 1 cm
11	02	Wood (thick)–Wood (thin)	3.5 m and 2.5 m	Thick wood: 50 cm × 30 cm/2 cm Thin wood: 30 cm × 30 cm/1 cm
12	03	Metal Wood (Thick)-Wood (thin)	1.5 m	17.5 cm × 14.5 cm/ 1 cm, Thick wood: 50 cm × 30 cm/2 cm Thin wood: 30 cm × 30 cm/ 1 cm
13	03	Metal-Wood (Thick)-Wood (thin)	3.5 m, 2.5 m, 1.5 m	17.5 cm × 14.5 cm/ 1 cm, Thick wood: 50 cm × 30 cm/2 cm Thin wood: 30 cm × 30 cm/1 cm

TWI scanning methods—In TWI, three types of scanning are done for target detection and shape identification. The A-Scan or range profile is a dimensional plot, which provides information about the presence of a target along with the approximate location. The B-Scan gives information about a number of targets present in the down-range and the C-scan gives information about shape, height, and width. A-Scan plots for different target ID are shown in Figure A1. B-Scan and C-Scan images are developed using 30 horizontal scans and 15 vertical scans.

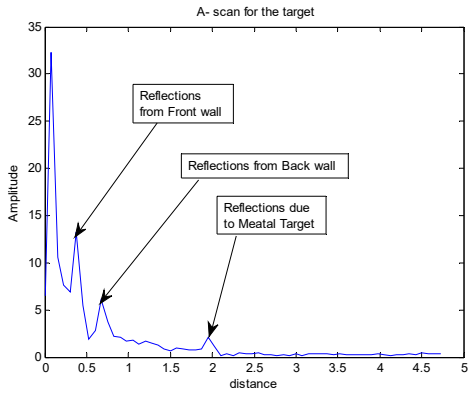

Target ID 01

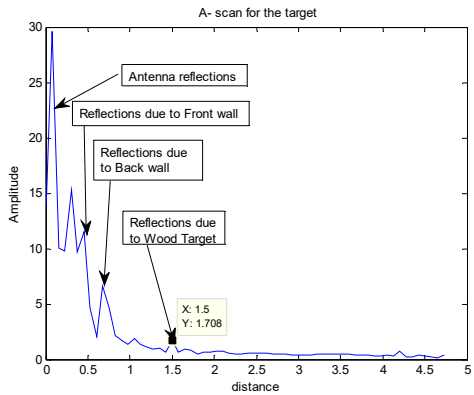

Target ID 02

Figure A1. *Cont.*

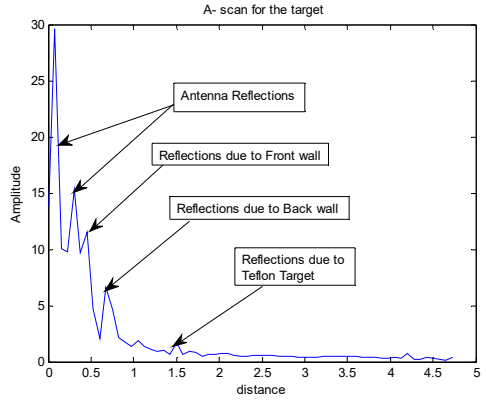

Target ID 03

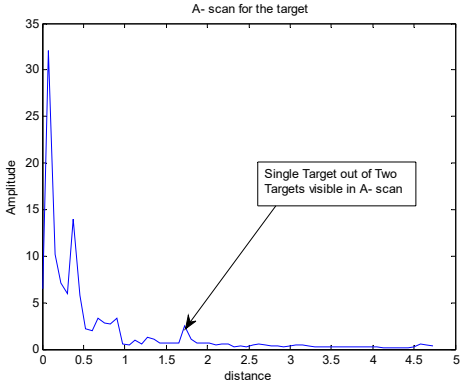

Target ID 13

Figure A1. A-scan of different target set-up.

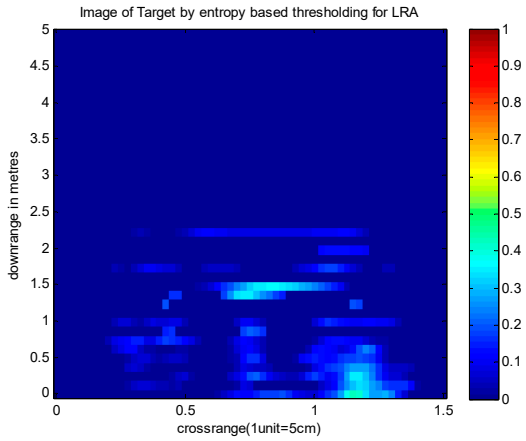

Target ID 03

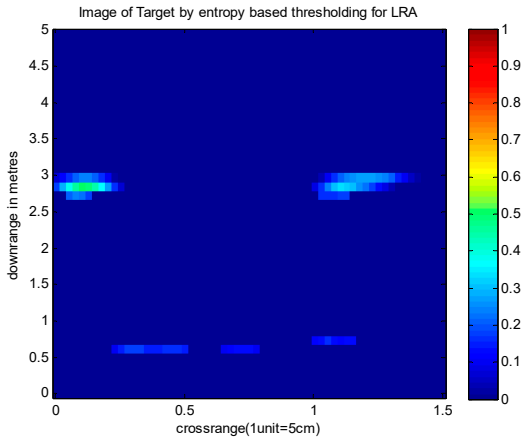

Target ID 04

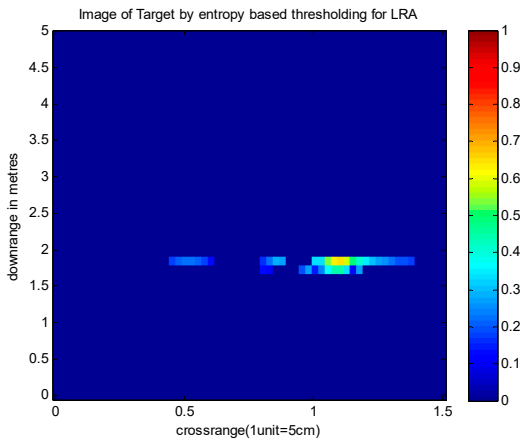

Target ID 06

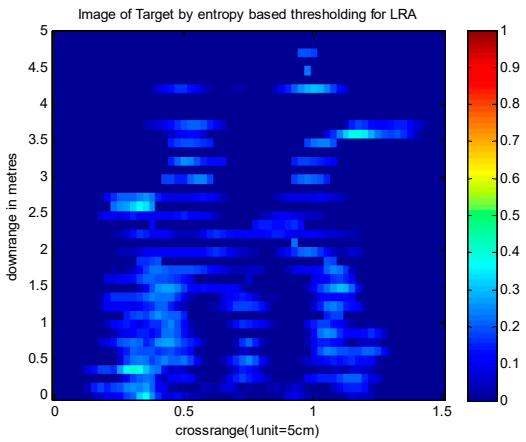

Target ID 11

Figure A2. *Cont*.

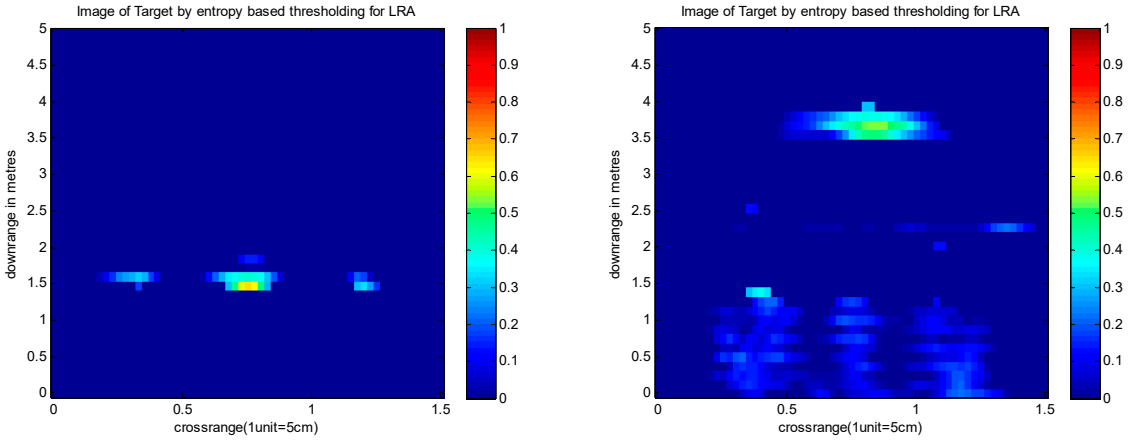

Target ID 12 Target ID 13

Figure A2. B-scan images for different targets.

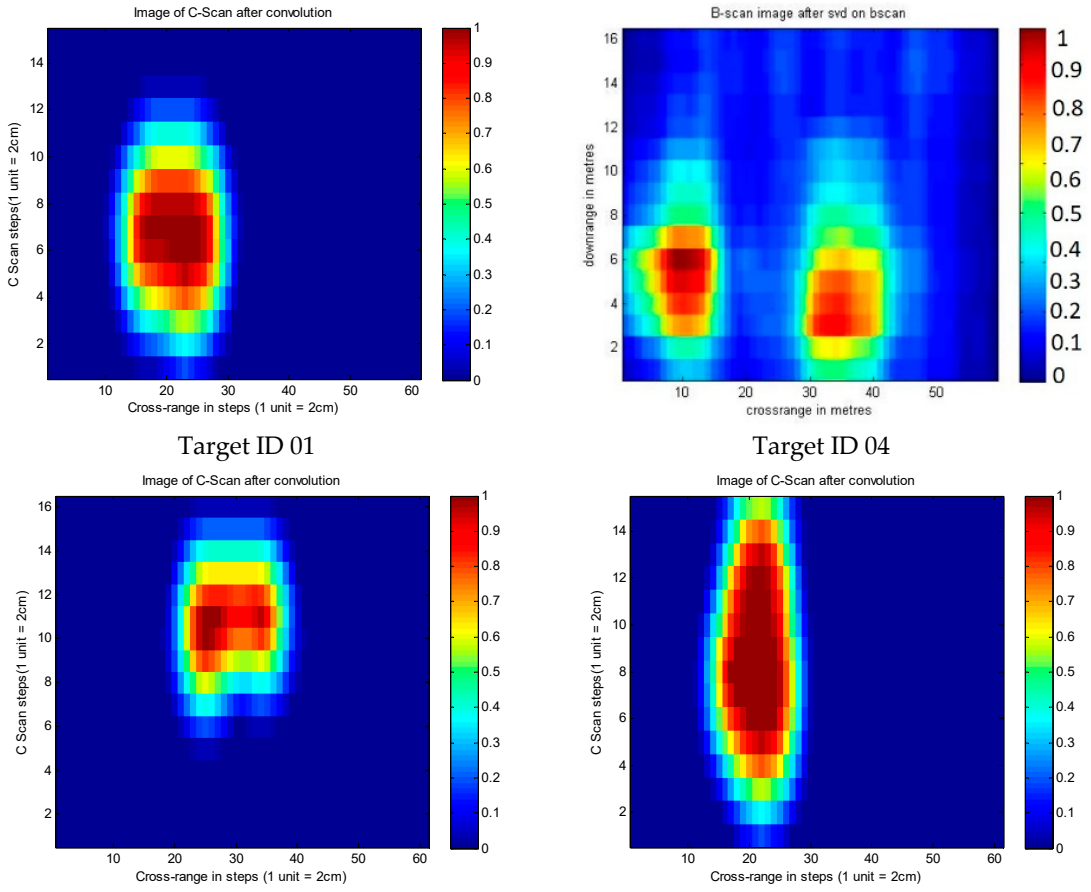

Target ID 01 Target ID 04

Target ID 03 Target ID 02

Figure A3. C-scan images for different targets where the color bar represents normalized intensity values.

References

1. Verma, P.K.; Gaikwad, A.N.; Singh, D.; Nigam, M.J. Analysis of Clutter Reduction Techniques for through Wall Imaging in UWB Range. *Prog. Electromagn. Res.* **2009**, *17*, 29–48. [CrossRef]
2. Potin, D.; Duflos, E.; Vanheeghe, P. Landmines Ground-Penetrating Radar Signal Enhancement by Digital Filtering. *IEEE Trans. Geosci. Remote Sens.* **2006**, *44*, 2393–2406. [CrossRef]
3. van der Merwe, A.; Gupta, I.J. A novel signal processing technique for clutter reduction in GPR measurements of small, shallow land mines. *IEEE Trans. Geosci. Remote Sens.* **2000**, *38*, 2627–2637.

4. Daniels, D.J. A review of landmine detection using GPR. In Proceedings of the 2008 European Radar Conference, Amsterdam, Netherlands, 30–31 October 2008; pp. 280–283.
5. van Kempen, L.; Sahli, H. Signal processing techniques for clutter parameters estimation and clutter removal in GPR data for landmine detection. In Proceedings of the 11th IEEE Signal Processing Workshop on Statistical Signal Processing (Cat. No.01TH8563), Singapore, 8 August 2001; pp. 158–161.
6. Zoubir, A.M.; Chant, I.J.; Brown, C.L.; Barkat, B.; Abeynayake, C. Signal processing techniques for landmine detection using impulse ground penetrating radar. *IEEE Sens. J.* **2002**, *2*, 41–51. [CrossRef]
7. Gaikwad, A.N.; Singh, D.; Nigam, M.J. Application of clutter reduction techniques for detection of metallic and low dielectric target behind the brick wall by stepped frequency continuous wave radar in ultra-wideband range. *IET Radar Sonar Navig.* **2011**, *5*, 416–425. [CrossRef]
8. Tivive, F.H.C.; Bouzerdoum, A.; Amin, M.G. A Subspace Projection Approach for Wall Clutter Mitigation in Through-the-Wall Radar Imaging. *IEEE Trans. Geosci. Remote Sens.* **2015**, *53*, 2108–2122. [CrossRef]
9. Tebchrany, E.; Sagnard, F.; Baltazart, V.; Tarel, J.; Dérobert, X. Assessment of statistical-based clutter reduction techniques on ground-coupled GPR data for the detection of buried objects in soils. In Proceedings of the 15th International Conference on Ground Penetrating Radar, Brussels, Belgium, 30 June–4 July 2014; pp. 604–609.
10. Tivive, F.H.C.; Bouzerdoum, A.; Amin, M.G. An SVD-based approach for mitigating wall reflections in through-the-wall radar imaging. In Proceedings of the 2011 IEEE RadarCon (RADAR), Kansas City, MO, USA, 23–27 May 2011; pp. 519–524.
11. Tivive, F.H.C.; Amin, M.G.; Bouzerdoum, A. Wall clutter mitigation based on eigen-analysis in through-the-wall radar imaging. In Proceedings of the 2011 17th International Conference on Digital Signal Processing (DSP), Corfu, Greece, 6–8 July 2011; pp. 1–8.
12. Chen, Y.; Zhou, Y.; Chen, W.; Zu, S.; Huang, W.; Zhang, D. Empirical Low-Rank Approximation for Seismic Noise Attenuation. *IEEE Trans. Geosci. Remote Sens.* **2017**, *55*, 4696–4711. [CrossRef]
13. Mohsin Riaz, M.; Ghafoor, A. Through-Wall Image Enhancement Based on Singular Value Decomposition. Available online: https://www.hindawi.com/journals/ijap/2012/961829/ (accessed on 29 May 2018).
14. Zhang, Y.; Xia, T. In-Wall Clutter Suppression Based on Low-Rank and Sparse Representation for Through-the-Wall Radar. *IEEE Geosci. Remote Sens. Lett.* **2016**, *13*, 671–675. [CrossRef]
15. Wang, G.; Amin, M. A new approach for target location of through the wall radar imaging in the presence of wall ambiguities. In Proceedings of the Fourth IEEE International Symposium on Signal Processing and Information Technology, Rome, Italy, 18–21 December 2004; pp. 183–186.
16. Boje, E. Fast discrete Fourier transform with exponentially spaced points. *IEEE Trans. Signal Process.* **1995**, *43*, 3033–3035. [CrossRef]
17. Nicolaescu, I.; Genderen, P. van Procedures to improve the performances of a Sfcw radar used for landmine detection. In Proceedings of the 2008 Microwaves, Radar and Remote Sensing Symposium, Kiev, Ukraine, 22–24 September 2008; pp. 250–255.
18. Mikhnev, V.A.; Vainikainen, P. Single-reference near-field calibration procedure for step-frequency ground penetrating radar. *IEEE Trans. Geosci. Remote Sens.* **2003**, *41*, 75–80. [CrossRef]
19. Ahmad, F.; Amin, M.G.; Kassam, S.A. A beamforming approach to stepped-frequency synthetic aperture through-the-wall radar imaging. In Proceedings of the 1st IEEE International Workshop on Computational Advances in Multi-Sensor Adaptive Processing, Puerto Vallarta, Mexico, 13–15 December 2005; pp. 24–27.
20. Kaushal, S.; Kumar, B.; Singh, D. An autofocusing method for imaging the targets for TWI radar systems with correction of thickness and dielectric constant of wall. *Int. J. Microw. Wirel. Technol.* **2019**, *11*, 15–21. [CrossRef]
21. Yao, Q.; Qifu, W. Kirchoff Migration Algorithm for Ground Penetrating Radar Data. In Proceedings of the 2012 International Conference on Computer Science and Electronics Engineering, Hangzhou, China, 23–25 March 2012; Volume 2, pp. 396–398.
22. Yektakhah, B.; Dehmollaian, M. A Method for Cancellation of Clutter Due to an Object in Transceiver Side of a Wall for Through-Wall Sensing Applications. *IEEE Geosci. Remote Sens. Lett.* **2012**, *9*, 559–563. [CrossRef]
23. Kumar, B.; Upadhyay, R.; Singh, D. Development of an Adaptive Approach for Identification of Targets (Match Box, Pocket Diary and Cigarette Box) under the Cloth with MMW Imaging System. *Prog. Electromagn. Res.* **2017**, *77*, 37–55. [CrossRef]
24. Kumar, B.; Sharma, P.; Singh, D. Development of an efficient approach for MMW imaging system to identify concealed targets inside the book. *Microw. Opt. Technol. Lett.* **2017**, *59*, 2982–2990. [CrossRef]

25. Solimene, R.; Cuccaro, A. Front Wall Clutter Rejection Methods in TWI. *IEEE Geosci. Remote Sens. Lett.* **2014**, *11*, 1158–1162. [CrossRef]
26. Yoon, Y.S.; Amin, M.G. Spatial Filtering for Wall-Clutter Mitigation in Through-the-Wall Radar Imaging. *IEEE Trans. Geosci. Remote Sens.* **2009**, *47*, 3192–3208. [CrossRef]
27. Dehmollaian, M.; Thiel, M.; Sarabandi, K. Through-the-Wall Imaging Using Differential SAR. *IEEE Trans. Geosci. Remote Sens.* **2009**, *47*, 1289–1296. [CrossRef]
28. Hyvarinen, A. Fast and robust fixed-point algorithms for independent component analysis. *IEEE Trans. Neural Netw.* **1999**, *10*, 626–634. [CrossRef] [PubMed]
29. Stickley, G.F.; Noon, D.A.; Cherniakov, M.; Longstaff, I.D. Gated stepped-frequency ground penetrating radar. *J. Appl. Geophys.* **2000**, *43*, 259–269. [CrossRef]